Freezing of argon in ordered and disordered porous carbon

Benoit Coasne,[1,*] Surendra K. Jain,[2] Linda Naamar,[1] and Keith E. Gubbins[2]
[1]*Institut Charles Gerhardt Montpellier, CNRS and Université Montpellier 2, Place Eugène Bataillon, 34095 Montpellier Cedex 05, France*
[2]*Center for High Performance Simulation and Department of Chemical and Biomolecular Engineering, North Carolina State University, Raleigh, North Carolina 27695-7905, USA*
(Received 5 December 2006; revised manuscript received 3 June 2007; published 15 August 2007)

We report a molecular simulation study on the freezing of argon within two models of activated porous carbons. Model A is a regular slit-shaped nanopore, which represents an ordered graphitic porous carbon with a single pore width. Model B is a realistic sample of a disordered porous carbon obtained from reverse Monte Carlo. The morphological (pore shape) and topological (pore connectivity) disorders of model B represent in a realistic way the complex porous structure of materials obtained after carbonization and activation of pure saccharose. This study is aimed at estimating how the effect of disorder of the porous material affects freezing and melting of simple adsorbates. Freezing of argon in the slit pore model conforms to the classical behavior for an adsorbate confined in a strongly attractive pore; the in-pore freezing temperature is higher than that of the bulk fluid, and the shift in freezing temperature increases with decreasing pore size. It is found that the two-dimensional crystal layers of argon within the slit pores have a hexagonal structure (i.e., triangular symmetry). Freezing of argon within model B strongly departs from that observed for model A. No crystallization is observed for argon in the complex porosity of model B. Nevertheless the confined phase undergoes structural changes at a temperature $T=115$ K; this temperature is close to the freezing temperature found for the slit pore with width $H=1.1$ nm, which corresponds to the mean pore size in model B. For temperatures larger than $T=115$ K, the confined phase in model B exhibits a liquid-like behavior as revealed from pair correlation functions and bond-order parameters. On the other hand, the confined phase for $T<115$ K has more short-range order than the liquid phase but its overall behavior remains liquid-like. Our results indicate that the changes observed at $T\sim115$ K are due (1) to the appearance in the confined phase of a small amount of crystal atoms and (2) to the fact that the fraction of liquid-like atoms having at least seven nearest neighbors reaches a plateau value of 80%. The results provide a basis for the interpretation of experiments such as NMR and scattering experiments on freezing in disordered porous materials.

DOI: 10.1103/PhysRevB.76.085416 PACS number(s): 61.46.−w, 64.60.−i, 05.70.−a

I. INTRODUCTION

Activated porous carbons are microporous solids with pores having a width of several angstroms. These materials attract a great deal of attention because of their use in industry as adsorbents for gas separation or storage, air purification, solvent recovery, or as electrodes for electrochemical batteries.[1–4] Activated porous carbons are obtained using a two-stage process of carbonization and activation. Carbonization consists of pyrolizing some organic precursor (polymer, coconut shell, saccharose, wood, pitch, etc.) in an inert atmosphere.[1,2] Samples obtained after this first stage are usually poor adsorbents as most of their porosity consists of closed pores or open pores having a small width. The adsorption properties of these materials are then enhanced using physical (high temperature treatment in the presence of H_2O/CO_2 vapors) or chemical (reactions with acid compounds) activation, which increases the internal surface, widens the already existing pores, and forms new pores. The morphological (pore shape) and topological (the way pores connect in space) properties of these materials strongly depend on the initial precursor and on the activation conditions.[1,4] Precursors such as polymers or pitch fibers, which are easily graphitized under heat treatment, lead after activation to ordered porous materials made up of graphene microcrystals.[5–8] The porosity in these materials consists of well-ordered though defective slit domains that are located between the graphene sheets. On the other hand, nongraphitizing precursors such as wood, coconut, or saccharose lead to highly disordered porous structures with connected pores of a complex geometry.[1,4,9]

From a fundamental point of view, activated porous carbons are used to investigate the effect of confinement, reduced dimension, and surface forces on the thermodynamic properties of fluids. As a result, many experimental, molecular simulation, and theoretical works have been reported on the phase behavior of fluids confined in these materials (for recent reviews, see Refs. 10 and 11). In most simulation and theoretical studies, activated porous carbons are modeled as an assembly of structureless slit pores (i.e., without atomic surface corrugation) of a particular pore width. On the other hand, recent molecular simulation studies have investigated the behavior of fluids confined within atomistic models of defective[12] or disordered[9,13–16] porous carbon. In the case of gas adsorption,[13] we recently showed that the behavior of argon within a saccharose-based disordered porous carbon strongly departs from that observed for smooth slit pores.[13,17,18] As a result, it was found that the complex porous network of the disordered sample cannot be modeled as an assembly of unconnected pores of a simple geometry having the same pore size distribution. A similar difference between gas adsorption in ordered and disordered porous structures was also demonstrated in the case of silica

mesopores.[13,19–25] The effect of pore shape and pore connectivity on freezing and melting of confined fluids was also recently addressed in several papers.[14,26,27] Biggs *et al.*[14] used a model of disordered material that was initially developed by Oberlin *et al.*[28,29] to investigate the freezing of fluids confined in activated porous carbons. However, as noted by the authors in Ref. 14, it is not clear whether this model is an accurate representation of real materials. On the other hand, recent advances in modeling of porous carbons have been achieved through the use of constrained reverse Monte Carlo (RMC) algorithms[30] and realistic models of these materials are available.[9,15,31,32] For the case of saccharose based porous carbon, Gubbins and co-workers have shown that the structural models obtained using constrained RMC are in good agreement with experimental data in terms of transmission electronic microscopy, gas adsorption, and microcalorimetry.[9,16]

This paper reports a molecular simulation study of the freezing of argon within ordered (model A) and disordered (model B) porous carbons. The motivation for this work, a brief report of which was first given in Ref. 33, is to disentangle the effect of confinement and the effect of disorder of the porous structure on freezing and melting of simple adsorbates confined in activated porous carbons. Model A is a regular slit nanopore, which represents ordered graphitic porous carbons as obtained from carbonization and activation of polymers or pitch fibers. Model B is a realistic sample of disordered porous carbons obtained from constrained RMC.[15] The morphological (pore shape) and topological (pore connectivity) disorders of model B are representative of materials obtained after activation of saccharose-based porous carbons.[15] For the case of model A, three different pore sizes, $H=0.7$, 1.1, and 1.4 nm, were considered as they correspond to the smallest, mean, and largest pore size in model B, respectively. Freezing of the confined fluid was determined in both pore models using grand canonical Monte Carlo (GCMC) simulations combined with a parallel tempering technique. The structure of the confined fluid was analyzed using crystalline order parameters and positional or bond orientational pair correlation functions. The remainder of the paper is organized as follows. In Sec. II, we present the two models of porous carbon used in this work. We also briefly discuss the details of the simulation techniques. Section III presents results for freezing of argon in the ordered and disordered porous carbon. Section IV contains concluding remarks and suggestions for future work.

II. COMPUTATIONAL DETAILS

A. Models of microporous carbons

Two different pore models were considered in this work. Model A consists of unconnected slit pores having a regular pore width and structureless walls. Model B is a realistic sample that possesses the morphological and topological properties of disordered materials obtained after activation of saccharose-based porous carbons.

1. Ordered porous carbon (model A)

Ordered porous carbons were modeled as unconnected slit pores having a regular width. Three different pore widths were considered, $H=0.7$, 1.1, and 1.4 nm. The size of the square section was 6.81×6.81 nm^2, which corresponds to $20\sigma\times20\sigma$ (σ is the size of the argon atom). The parallel walls of the slit graphite pore were described as structureless, i.e., without atomic surface corrugation. We expect this approximation to be reasonable for argon as the size of this adsorbate, $\sigma\sim0.34$ nm, is much larger than the spacing between carbon atoms in graphite, $D\sim0.14$ nm. The interaction between the fluid and the pore walls was calculated using the Steele "10-4-3" potential:[34,35]

$$U_{\mathrm{wf}}(z)=2\pi\rho_w\varepsilon_{\mathrm{wf}}\sigma_{\mathrm{wf}}^2\Delta\left[\frac{2}{5}\left(\frac{\sigma_{\mathrm{wf}}}{z}\right)^{10}-\left(\frac{\sigma_{\mathrm{wf}}}{z}\right)^4-\left(\frac{\sigma_{\mathrm{wf}}^4}{3\Delta(z+0.61\Delta)^3}\right)\right], \quad (1)$$

where z is the distance between the adsorbed molecule and the graphite surface, Δ is the separation between graphite layers, 0.335 nm, and ρ_{w} the number density of carbon atoms within the graphitic layers, 114 nm^{-3}. The first and second terms in Eq. (1) are, respectively, the repulsive and attractive parts of the interaction between the adsorbed molecule and the graphite surface while the third term represents the summation over the other graphite layers.[34] The wall-fluid Lennard-Jones parameters $\varepsilon_{\mathrm{wf}}$ and σ_{wf} were determined by combining the wall-wall[35] (i.e., carbon-carbon) and fluid-fluid[36] (i.e., argon-argon) parameters using the Lorentz-Berthelot rules[37] (see Table I). In the case of a slit pore having a width H, the fluid interacts with both graphite surfaces and the total fluid-wall interaction is given by

$$V_{\mathrm{wf}}(z)=U_{\mathrm{wf}}(z)+U_{\mathrm{wf}}(H-z), \quad (2)$$

where $U_{\mathrm{wf}}(z)$ and $U_{\mathrm{wf}}(H-z)$ are calculated using Eq. (1). Radhakrishnan *et al.*[38,39] have shown that the parameter $\alpha=\rho_w\varepsilon_{\mathrm{wf}}\sigma_{\mathrm{wf}}^2\Delta/\varepsilon_{ff}$, i.e., the ratio of the wall-fluid to the fluid-fluid attractive interactions, can be used to predict the change in freezing temperature of a confined system having simple spherical molecules and simple pore geometry. An increase (decrease) in the freezing temperature compared to the bulk is expected for $\alpha>1$ ($\alpha<1$). For argon confined in graphite pores $\alpha=2.14$, so that we expect the in-pore freezing temperature to be larger than for the bulk.

TABLE I. Lennard-Jones parameters used to calculate the wall-fluid and fluid-fluid interactions.

Ar-Ar	$\sigma=0.3405$ nm	$\varepsilon/k=120.0$ K
C-C	$\sigma=0.336$ nm	$\varepsilon/k=28.0$ K
Ar-C	$\sigma=0.338$ nm	$\varepsilon/k=58.0$ K

2. Disordered porous carbon (model B)

The disordered porous structure considered in this work is a structural model of activated porous carbon obtained by Jain *et al.* using a constrained RMC method.[15] This method consists of generating atomic configurations that match the structural properties of the real system.[30] The quantity that must be minimized in the course of the simulation is the

difference between the simulated and experimental pair correlation functions:

$$\chi^2 = \sum_{i=1}^{n} [g_{\mathrm{sim}}(r_i) - g_{\mathrm{exp}}(r_i)]^2. \quad (3)$$

The uniqueness theorem in statistical mechanics[40,41] states that structures determined by RMC in which only pair correlation functions are considered are not unique if many body forces exist in the system (as in the case of carbon structures for which chemical bonding is involved). In other words, many body forces must be somehow included in the simulation in order to specify the system in a complete manner. Following the previous work by Pikunic *et al.*,[16] appropriate constraints were used to build the realistic model of activated porous carbon used in this work. The first constraint is that the fraction of atoms having sp^2 hybridization (i.e., coordination number of 3) must be equal to that determined from the experimental composition [Eq. (4)]. The second constraint is that the average C-C-C bond angle must be equal to $2\pi/3$, as expected for sp^2 hybridization [Eq. (5)]:

$$\delta^2 = \left[\left(\frac{N_3}{N} \right)_{\mathrm{sim}} - \left(\frac{N_3}{N} \right)_{\mathrm{exp}} \right]^2, \quad (4)$$

$$\Psi^2 = \frac{1}{n} \sum_{\theta_i=1}^{n_\theta} \left[\cos(\theta_i) - \cos\left(\frac{2\pi}{3} \right) \right]^2, \quad (5)$$

where N_3 is the number of C atoms being three-coordinated while N is the total number of atoms. θ_i and n_θ are the value of a given C-C-C bond angle and the total number of C-C-C angles in the system, respectively.

In the constrained RMC simulation, the difference χ^2 between the experimental and simulated pair correlation functions are simultaneously minimized with the two constraints δ^2 and Ψ^2. Changes in the atomic configurations are accepted or rejected according to the Metropolis acceptance probability:

$$P_{\mathrm{acc}} = \min\left[1, \exp\left\{ -\frac{1}{T_\chi}(\chi^2_{\mathrm{new}} - \chi^2_{\mathrm{old}}) - \frac{1}{T_\delta}(\delta^2_{\mathrm{new}} - \delta^2_{\mathrm{old}}) - \frac{1}{T_\Psi}(\Psi^2_{\mathrm{new}} - \Psi^2_{\mathrm{old}}) \right\} \right], \quad (6)$$

where T_χ, T_δ, and T_Ψ are weighting parameters. In order to improve the quality of the sampling in the constrained RMC simulation, the method was combined with a simulated annealing technique. The latter is a minimization technique that consists of first melting the structure to be optimized at high temperature and then slowly lowering the temperature. Starting with a random initial structure at high temperature, the system runs at this temperature for a large number of moves until it reaches equilibrium; each move consists of randomly selecting and displacing a C atom to a new position. Then the temperature is decreased and the system is again allowed to come to equilibrium at this new temperature. The simulation is complete when no further change is observed upon decrease of the temperature. Full details of the simulation techniques can be found in Refs. 9 and 15.

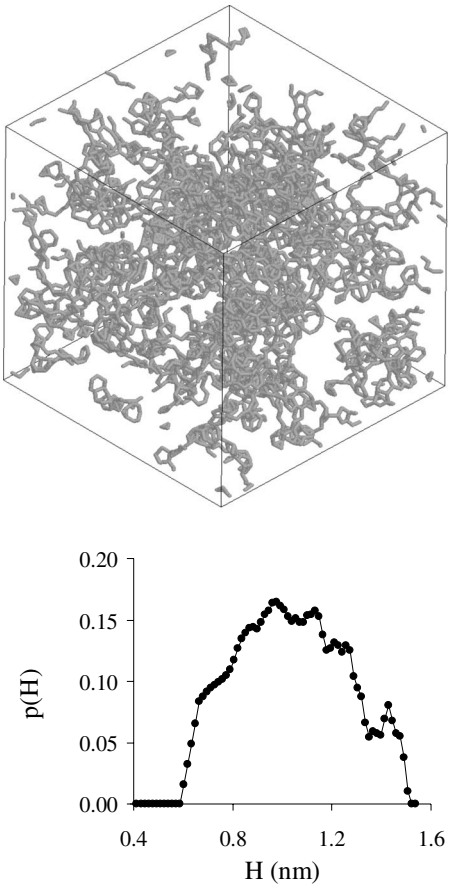

FIG. 1. (Top) Snapshot of the structural model of activated porous carbon CS1000A obtained using a constrained reverse Monte Carlo method [from Jain *et al.* (Ref. 15)]. The box size is 5 nm. The gray sticks represent the C-C bonds. (Bottom) Pore size distribution of the activated porous carbon shown on the left.

The disordered porous carbon used in this work, named CS1000A, corresponds to the porous structure obtained after activation of a coke sample that was produced by pyrolizing pure saccharose at 1000 °C under nitrogen flow. The activation process corresponds to a heat treatment in a CO_2 atmosphere for 20 h. The density of carbon atoms in the CS1000A structure is 0.722 mg/ml. A snapshot of the configuration of CS1000A is shown in Fig. 1. The size of the box used to generate this numerical sample of disordered porous carbon is $5 \times 5 \times 5$ nm^3. Following the previous work by Gelb and Gubbins,[42] the pore size distribution of the sample was calculated as follows. $p(H)dH$ is the fraction of pore volume that is occupied by pores in the range H and $H+dH$. The pore size distribution has a mean value of about 1.1 nm with a broad dispersion of ±0.5 nm (Fig. 1).

B. Grand canonical Monte Carlo simulation

Freezing of argon within the different models of activated porous carbons was simulated using the GCMC algorithm. The GCMC technique is a stochastic method that simulates a system having a constant volume V (the pore with the adsorbed phase), in equilibrium with an infinite fictitious reservoir of particles imposing its chemical potential μ and its

temperature T.[43–45] The density of the confined phase is obtained from the ensemble average of the number of adsorbed atoms. Periodic boundary conditions were used in the three directions (x,y,z) in order to avoid finite-size effect for the disordered porous system CS1000A (model B). On the other hand, periodic boundary conditions were applied only in the directions (x,y) parallel to the pore walls for the slit pore model (model A). As mentioned in Sec. II A, interactions between Ar and the slit pore walls for model A were calculated using the 10-4-3 Steele potential given by Eq. (1). The interaction of argon atoms with the carbon atoms of the disordered porous material were modeled using a Lennard-Jones potential; the fluid-fluid and fluid-wall parameters were the same as those used for the slit pore model (Table I). In order to accelerate the simulations in the case of CS1000A (model B), the adsorbate-substrate interaction was calculated by using an energy grid;[46] the potential energy is calculated at each corner of each elementary cube (about $0.025 \times 0.025 \times 0.025$ nm^3). An accurate estimation of the energy is then obtained by a linear interpolation of the grid values. This procedure enables simulation of adsorption in nanoporous media of complex morphology and/or topology without a direct summation over matrix species in the course of GCMC runs.[22,23,25,47–49] The Ar-Ar interactions were calculated using Lennard-Jones potentials with the parameters reported in Table (1).[36]

Simulations of argon confined in the porous materials were performed at constant fugacity f, which corresponds to that of an ideal gas phase at a pressure $P=1$ atm. This choice of thermodynamic condition avoids the problem of having to determine the chemical potential in the bulk phase at and near the freezing point. However, the pressure of the reservoir will vary with temperature as the bulk phase departs from the ideal gas state when the temperature is changed; we do not expect the pressure variation to have a large effect on the freezing behavior, as evidenced by results for bulk systems. In order to circumvent the difficulty of particle deletion and insertion in dense phases such as liquids and solids, the GCMC simulations were combined with the parallel tempering technique.[45,50,51] This method consists of considering several replicas of the system at different temperatures and chemical potentials. In addition to conventional Monte Carlo moves that are performed for each replica, trial swap moves between configurations in different replicas are attempted. The parallel tempering technique prevents the system from being "trapped" in local metastable states.[27,52–56] Full details of the GCMC and parallel tempering techniques used in this work have been described elsewhere.[52] Twelve replicas were used in this work for both the ordered and disordered porous structures. The temperature difference between two successive replicas is $\Delta T=4$ K for the slit pore model. As no significant crystallization was observed for argon in the CS1000A structure (see below), we used a larger temperature difference for this system, $\Delta T=6$ K. We started with well-equilibrated liquid configurations of the confined fluid and performed, at least, 10^5 Monte Carlo steps per particle to equilibrate the system using the parallel tempering technique. After equilibration of the system, density profiles, bond order parameters, and pair correlation functions were averaged in the course of a second simulation run.

Strong layering of Ar was observed for the slit pore model, due to the interaction with the attractive pore walls. Following previous works on freezing in slit nanopores,[27,39,56–58] the structure of the confined fluid was investigated by calculating for each adsorbate layer i the 2D bond-order parameters $\Phi_{6,i}$. We determined $\Phi_{6,i}$ as the average value of the local order parameter $\Psi_{6,i}(\mathrm{r})$, which measures the hexagonal bond order at a position $\mathbf{r}$ of a particle located in the layer i:[59,60]

$$\Phi_{6,i} = \frac{\left| \int \Psi_{6,i}(\mathbf{r}) d\mathbf{r} \right|}{\int dr} \text{ with } \Psi_{6,i}(\mathbf{r}) = \frac{1}{N_b} \sum_{k=1}^{N_b} \exp(i6\theta_k), \tag{7}$$

where θ_k are the bond angles between the particle and each of its N_b nearest neighbors. $\Phi_{6,i}$ is close to 1 for a crystal layer having a hexagonal structure (i.e., triangular symmetry) and close to 0 for a liquid layer. We also monitored for each adsorbate layer the two-dimensional (2D) in-plane positional and bond-orientational pair correlation functions, $g_i(\mathrm{r})$ and $G_{6,i}(\mathrm{r})$.[38,39,52,58,61] The latter measures for each layer i the correlations between the local bond order parameter $\Psi_{6,\mathrm{j}}(\mathrm{r})$ at two positions separated by a distance r:

$$G_{6.i}(r) = \langle \Psi^*_{6,i}(0) \Psi_{6,i}(r) \rangle. \tag{8}$$

Properties of Ar confined in the slit pore are identical along the x and y directions, due to the 2D geometry for this model. In contrast, the porosity of CS1000A is isotropic (i.e., x, y, and z directions are equivalent), so that the structure of the confined fluid was analyzed using 3D pair correlation functions g(r) and 3D bond-orientational order parameters Q_4 and Q_6:[62]

$$Q_l = \left[\frac{4\pi}{2l+1} \sum_{m=-l}^{l} |\bar{Q}_{lm}|^2 \right]^{1/2} \tag{9}$$

with

$$\bar{Q}_{lm} = \frac{1}{N_b} \sum_{i=1}^{N_b} Y_{lm}(\theta_i, \phi_i), \tag{10}$$

where N_b is the total number of nearest-neighbor bonds in the system. θ_i and φ_i are the polar and azimuthal angles giving the orientation of a given nearest-neighbor bond and Y_{lm} are spherical harmonics.[63] The order parameters Q_6 and Q_4 can be used to determine any crystalline structure as they are sensitive to any orientational order by measuring the coherence of the local bond order of the atoms.[64,65] The components $\bar{Q}_{lm}$ in Eq. (10) add up in a coherent manner for a crystal as the angular part of the spherical harmonics are in phase; consequently, the resulting Q_l has a nonzero value that is characteristic of the crystal structure (on the other hand, Q_l is equal to 0 for a liquid phase as the components $\bar{Q}_{lm}$ add up in an incoherent manner).[66] As a result, we found that these order parameters are not suitable to study freezing of argon in CS1000A (model B) as the large degree of disorder in this

porous sample prevents the orientational order of the confined phase from being coherent. Thus, instead of calculating the global order parameters Q_4 and Q_6, we followed the work by ten Wolde *et al.*[66] who proposed to use *local* order parameters to distinguish particles that are liquid-like or crystal-like. For each atom i of the confined phase, we calculated the 13 normalized parameters $\tilde{q}_{6m}(i)$ that are defined as

$$\tilde{q}_{6m}(i) = \frac{A}{N_b(i)} \sum_{j=1}^{N_b(i)} Y_{6m}(\mathbf{r}_{ij}) \text{ with } m \in [-6,6], \quad (11)$$

where $\mathbf{r}_{ij}$ are the vectors joining the atom i and each of its $N_b(i)$ neighbors j. $A=[\Sigma_{m=-6}^{6}|\overline{q_{6m}}(i)|^2]^{-1/2}$ is the normalization constant. In contrast to $\bar{Q}_{lm}$ in Eq. (10), $\tilde{q}_{6m}(i)$ is a local quantity that depends only on atom i and its neighbors j. For each pair of nearest neighbors, we define the following scalar product:[66]

$$\mathbf{q}_6(i) \cdot \mathbf{q}_6(j) = \sum_{m=-6}^{6} \tilde{q}_{6m}(i)\tilde{q}_{6m}(j)^*. \quad (12)$$

Atoms i and j can be considered "connected" in a coherent manner if the product $\mathbf{q}_6(i)\cdot\mathbf{q}_6(j)$ is larger or equal to 0.5. ten Wolde *et al.* have shown that an atom i in a 3D environment is crystal-like if it is connected in a coherent manner to at least seven of its nearest neighbors; this definition ensures that liquid and bcc or fcc crystal structures are unambiguously distinguished.[66]

III. RESULTS AND DISCUSSION

A. Ordered porous carbon

1. Effect of confinement on freezing

Freezing of argon in graphite slit pores (model A) was studied for three different pore sizes, $H=0.7$, 1.1, and 1.4 nm. These pore widths were selected as they correspond to the smallest, the mean, and the largest pore size of the disordered porous carbon CS1000A (see Fig. 1). Density profiles of argon confined in the three slit pores is shown in Fig. 2 for $T=110$ K. Z^* and ρ^* are the distance from the center of the pore and the density in reduced units with respect to σ. Strong layering of argon is observed for each pore size; 2D layers are clearly separated by a minimum value of the density, $\rho^*=0$. The slit pores $H=0.7$ and 1.1 nm accommodate, respectively, one and two layers, while the slit pore $H=1.4$ nm accommodates two contact and one inner layer. It is found that the peak amplitude for the inner layer is lower than that for the contact layers. This result shows that the contact layers are more ordered than the inner layer, due to its stronger interaction with the pore wall.

A detailed analysis of the freezing of argon in the slit pore $H=1.4$ nm is reported in what follows. Results for the other slit pores will be summarized at the end of this section. The 2D bond-order parameter Φ_6 for the contact and inner layers of argon in the $H=1.4$ nm slit pore is reported as a function of the temperature T in Fig. 3. Φ_6 for the contact and inner layers sharply increases at $T\sim 112$ K upon freezing, which

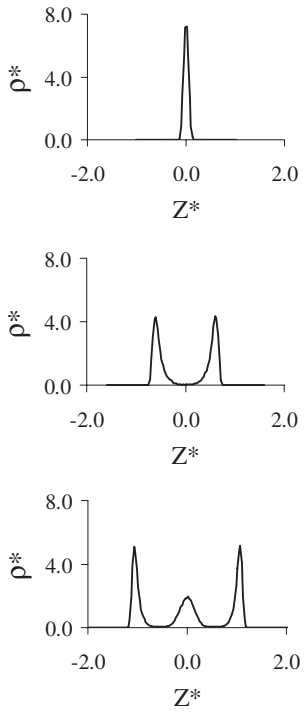

FIG. 2. Density profiles of Ar confined at $T=110$ K in a graphite slit pore of width: $H=0.7$ nm (top), $H=1.1$ nm (middle), and $H=1.4$ nm (bottom). Z^* is the distance from the center of the pore in reduced units with respect to σ. $\rho^*=\rho\sigma^3$ is the reduced density with respect to σ.

reveals that both layers undergo a liquid to crystal phase transition at this temperature. Φ_6 varies from ~ 0.1 in the liquid region up to ~ 0.8 in the crystal region; the latter value shows that the layers have a hexagonal crystal structure (triangular symmetry) with, however, some defects. The confined layers freeze at the same temperature, indicating that there is no significant difference in the freezing behavior of the contact and inner layers for this pore size. This result is in agreement with previous molecular simulation studies, which have shown that all the adsorbate freezes at the same temperature for slit pores accommodating three layers or less.[39,52,53,67] The global density of argon in the $H=1.4$ nm slit pore is shown in Fig. 3 as a function of the temperature T. The density decreases from $\rho^*\sim 1.1$ down to $\rho^*=1.0$ at $T=112$ K. This result corroborates our previous finding that structural modifications occur in the confined layers at $T\sim 112$ K. The observation of a sudden increase in the density and the bond-order parameter Φ_6 suggest that crystallization of the confined layers is a first-order transition. However, further study including free energy calculation is required to establish in a rigorous way the order of the crystal-to-liquid phase transition.[27,39,57] Thanks to the use of the parallel tempering technique in which both the liquid and crystal phases are simulated in the same run, we did not perform calculations for the melting process. In our previous works,[52,68] it was shown that simulations of melting and freezing phenomena give similar results, provided that the parallel tempering method is used and a significant fraction of the swap trial moves are accepted.[50,51] Moreover, Hung *et al.*[58] have shown for fluids confined in carbon nanotubes that this technique

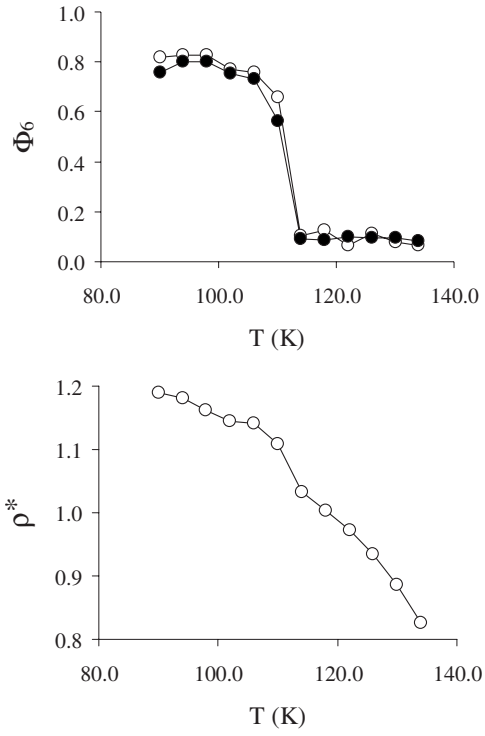

FIG. 3. (Top) Average value of the 2D bond-order parameter Φ_6 as a function of the temperature T for Ar confined in a slit graphite pore $H=1.4$ nm. Open and closed symbols are for the contact and inner layers, respectively. (Bottom) Reduced density $\rho^*=\rho\sigma^3$ as a function of the temperature T for Ar confined in a slit graphite pore $H=1.4$ nm.

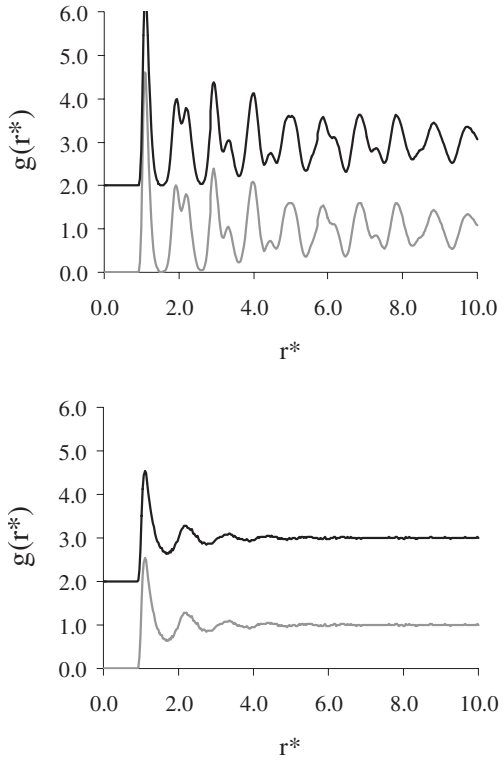

FIG. 4. In-plane 2D positional pair correlation function $g(r^*)$ for the contact (gray line) and inner (black line) layers of Ar confined in a slit graphite pore $H=1.4$ nm at T=94 K (top) and at T=122 K (bottom). The $g(r^*)$ functions for the inner layer have been shifted by +2.0 for the sake of clarity. r^* is the reduced distance with respect to σ.

gives the same results as those obtained from free energy calculations.

2. Structure of confined fluid

In-plane 2D positional g(r) and orientational $G_6(r)$ pair correlation functions for the confined layers at $T=94$ and 122 K are presented in Figs. 4 and 5, respectively. Correlations within each layer were determined up to a distance of half the size of the simulation box. At $T=122$ K, the confined layers exhibit a liquid-like behavior as revealed by the g(r) function, which is characteristic of a phase having short-range positional order. This result is confirmed by the exponential decay observed in the $G_6(r)$ function; such a decay is typical of 2D liquid phases, which have short-range orientational order. At $T=94$ K, the confined layers appear as 2D hexagonal crystals with long-range positional order as can be seen from the features of the g(r) function for this temperature (Fig. 4): (i) the amplitude between the first and the second peak is close to 0; (ii) the second peak is split into two secondary peaks; and (iii) the third peak presents a shoulder on its right side. Moreover, the $G_6(r)$ function at this temperature has a constant average value as expected for a hexagonal crystal layer with long-range orientational order. Analysis of the in-plane 2D pair correlation functions g(r) and $G_6(r)$ corroborate the results shown in Fig. 3 for the 2D bond-order parameter Φ_6 and the density ρ^*; the transition temperature between the crystal and liquid phases is about $T=112\pm2$ K. It seems that freezing of the confined layers involves a direct phase transition between a 2D crystal and a 2D liquid. This result departs from previous molecular simulation and experimental works in which the existence of a hexatic phase between the crystal and liquid phases was reported.[69,70] Such an intermediate phase is expected according to the theory by Kosterlitz-Thouless-Halperin-Nelson-Young for the melting of 2D systems.[59,60,71,72] The stability of the hexatic phase depends on the size of the system, so that the existence of such an intermediate phase cannot be ruled out or confirmed in the present work unless a scaling size analysis is performed.[69]

3. Effect of pore size

The freezing temperature $T=112$ K of argon in the $H=1.4$ nm slit pore is much larger than that of bulk argon, $T=83$ K. This increase in the freezing temperature was expected as we know from previous experimental and theoretical works that fluids confined in strongly attractive pores may crystallize at higher temperature than the bulk.[11,38,39] Table II summarizes the freezing temperature for argon confined in the different slit pores $H=0.7$, 1.1, and 1.4 nm. An increase in the freezing temperature compared to the bulk is observed for all pore sizes. The shift in freezing temperature increases as the pore size decreases, as expected.[11,73,74] For all pore sizes, the confined layers of argon undergo at the

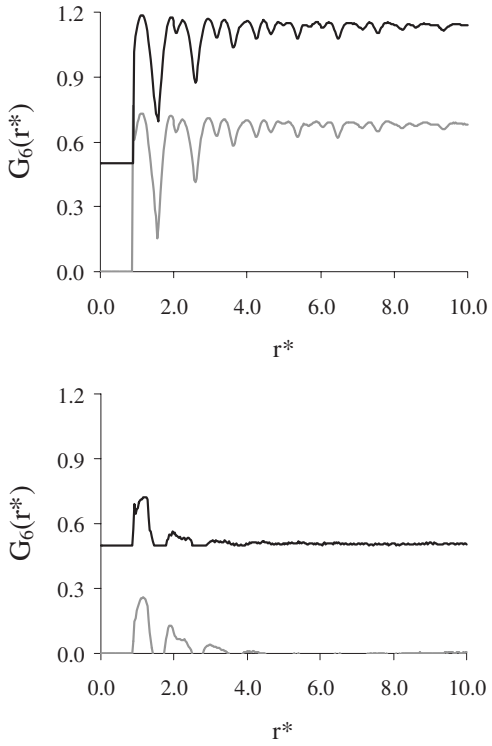

FIG. 5. In-plane 2D orientational pair correlation function $G_6(r^*)$ for the contact (gray line) and inner (black line) layers of Ar confined in a slit graphite pore $H=1.4$ nm at T=94 K (top) and at T=122 K (bottom). The $G_6(r^*)$ functions for the inner layer have been shifted by +0.5 for the sake of clarity. r^* is the reduced distance with respect to σ.

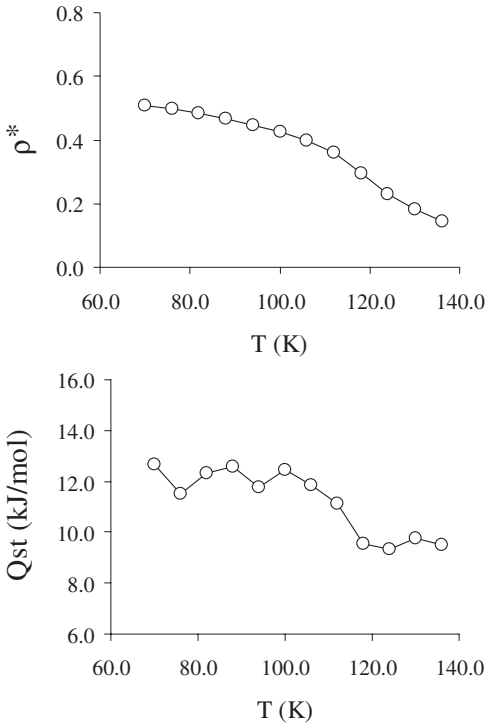

FIG. 6. (Top) Reduced density $\rho^*\rho\sigma^3$ of Ar confined in the activated porous carbon CS1000A as a function of the temperature T. (Bottom) Isosteric heat of adsorption Q_{st} of Ar confined in the activated porous carbon CS1000A as a function of the temperature T.

freezing temperature a phase transition between a 2D liquid-like structure and a 2D crystal layer having a hexagonal structure.

B. Disordered porous carbon

1. Effect of disorder on freezing

In order to study the effect of disorder of the porous material on the freezing of confined fluids, we simulated the behavior of argon at different temperatures in CS1000A. The density of argon in this porous structure is shown in Fig. 6 as a function of the temperature T. A change in the evolution of the density with temperature is observed for $T\approx 115$ K; ρ^* is almost constant about 0.4 to 0.5 for $T<115$ K, while ρ^* decreases more rapidly with increasing temperature for $T>115$ K. As shown in Fig. 6, this change in the variation of the density at $T\sim 115$ K is accompanied by a decrease from 11.1 to 9.6 kJ/mol of the isosteric heat of adsorption of argon in the porous material. The latter quantity was calculated in the GCMC simulations from the fluctuations over the energy and number of particles according to the following formula:[43]

$$q_{st} = k_B T - \frac{\partial\langle U\rangle}{\partial\langle N\rangle} \sim k_B T - \frac{\langle UN\rangle - \langle U\rangle\langle N\rangle}{\langle N^2\rangle - \langle N\rangle^2}. \qquad (13)$$

Both the change in the density and isosteric heat of adsorption indicate that argon confined within CS1000A undergoes structural modifications at $T\approx 115$ K. Interestingly, this temperature is very close to the freezing temperature for the slit pore $H=1.1$ nm (see Table II), which corresponds to the mean pore size of the disordered porous structure. This result suggests that the freezing behavior of argon confined in CS1000A is driven by the mean pore size of the sample. However, further calculations for other disordered porous carbon are needed to confirm this finding.

TABLE II. Freezing temperature of argon confined in slit pores of width $H=0.7$, 1.1, and 1.4 nm. The freezing temperature of bulk argon is 83 K. ΔT_f is the shift in freezing temperature between confined and bulk argon.

H (nm)	$T_{f,confined}$ (K)	ΔT_f (K)
0.7	140	57
1.1	116	33
1.4	112	29

2. Structure of confined fluid

In order to gain some insights on the nature of the change observed at $T\approx 115$ K, pair correlation functions g(r) of confined argon were calculated for each temperature (Fig. 7). Both the g(r) function at $T=70$ and 136 K are characteristic of liquid-like structures as only short-range positional order

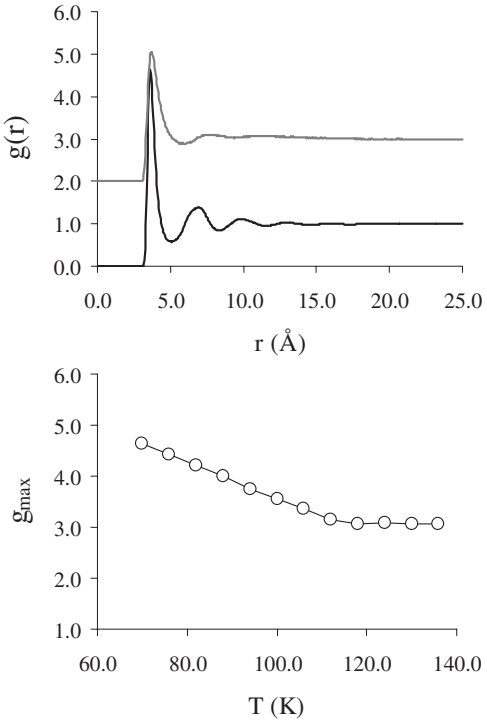

FIG. 7. (Top) Positional pair correlation function g(r) for Ar confined in the activated porous carbon CS1000A at $T=70$ K (black line) and $T=136$ K (gray line). The g(r) function for $T=136$ K has been shifted by +2.0 for the sake of clarity. (Bottom) Maximum value (first peak) of the function g(r) as a function of the temperature T for Ar confined in the activated porous carbon CS1000A.

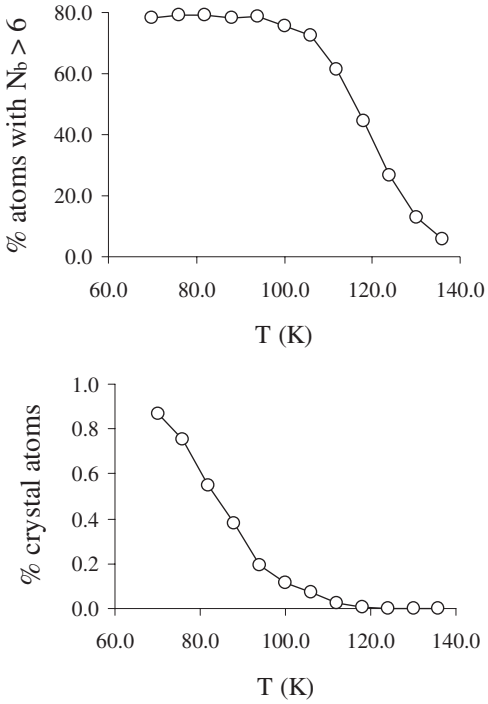

FIG. 8. (Top) Percentage of atoms having at least six nearest neighbors as a function of the temperature T for Ar confined in the activated porous carbon CS1000A (see text). (Bottom) Percentage of crystal-like atoms as a function of the temperature T for Ar confined in the activated porous carbon CS1000A (see text).

is observed. The maximum value of the g(r) function, which corresponds to the amplitude of the nearest-neighbor peak, is reported in Fig. 7 as a function of the temperature. The maximum value is constant at about $g_{max}=3$ for $T>115$ K; this value is close to that expected for a bulk fluid. On the other hand, g_{max} increases linearly with decreasing temperature for $T<115$ K. Such an analysis based on the positional pair correlation functions indicates that short-range structural modifications of argon in CS1000A occur at $T\approx 115$ K. However, it must be emphasized that the g(r) function is characteristic of a liquid-like structure for all temperatures. On the other hand, the augmentation in g_{max} with decreasing temperature indicates that the confined phase presents more short-range order for $T<115$ K, although it remains liquid-like overall.

In order to further characterize the structure of argon confined in CS1000A, the percentage of atoms having more than six nearest neighbors was calculated as a function of the temperature T (Fig. 8). The choice of this limit comes from the fact $N_b>6$ for the fcc and bcc crystals while $N_b\leqslant 6$ for the liquid phase, so that this criterion can be used to distinguish particles that are crystal-like and particles that are liquid-like. The percentage of atoms with $N_b>6$ reaches a plateau value of 80% for $T<115$ K. This result is consistent with the changes observed at this temperature in the pair correlation function, density of the confined phase, and isosteric heat of adsorption.

We also report in Fig. 8 the percentage of atoms that are crystal-like as a function of the temperature T. This quantity was determined using the order parameter $\mathbf{q}_6(i)\cdot\mathbf{q}_6(j)$ from the number of Ar atoms that are connected in a crystalline manner to its nearest neighbors (see Sec. II B for full details). We note that these crystal-like atoms are a subgroup of the particles with $N_b>6$. The fraction of crystal-like atoms is very small in the confined phase ($<1\%$). However, the temperature at which the number of crystal-like atoms drops to zero ($T\sim 115$ K) is consistent with the changes observed at this temperature in the pair correlation function, density of the confined phase, and isosteric heat of adsorption. This result indicates that the confined phase for $T<115$ K is a mixture of a small amount of crystalline atoms and amorphous (liquid or solid) regions. Such an observation is supported by previous molecular simulations and experiments on molecular fluids confined in cylindrical silica or carbon pores.[58,75,76] These authors have found that the confined fluid does not crystallize but forms an inhomogeneous phase composed of nanometric crystallites and amorphous regions.

IV. CONCLUSION

Freezing of argon in the slit pore model (model A) shows that the in-pore freezing temperature is higher than that of the bulk. It is also found that the shift in freezing temperature increases with decreasing the pore size, in agreement with previous molecular simulations and experiments on adsorbate confined in strongly attractive pores. Upon freezing the confined layers undergo a phase transition from a 2D liquid state to a hexagonal crystal state (i.e., triangular symmetry).

Freezing of argon within the disordered porous structure (model B) strongly departs from that observed for the simple slit pore model. Our results indicate that argon in the complex porosity of this porous model does not crystallize. Nevertheless, the confined phase undergoes structural changes at $T \sim 115$ K. Interestingly, this temperature is very close to the freezing temperature observed for the slit pore of width $H = 1.1$ nm, which corresponds to the mean pore size of the disordered porous structure. This result suggests that the freezing behavior of argon confined in this material is driven by the mean pore size of the sample. For $T > 115$ K, the confined phase in model B presents a liquid-like behavior, as revealed by pair correlation functions and bond-order parameters. On the other hand, the confined phase for $T < 115$ K has more short-range order than the liquid phase but its overall behavior remains liquid-like. We further analyzed the structure of the confined phase by determining the percentage of atoms having more than six nearest neighbors and the percentage of atoms that are crystal-like. A small amount of crystal atoms appears at $T \sim 115$ K. It is also found that the percentage of atoms with $N_b > 6$ reaches a plateau value of 80% below this temperature. This result shows that the confined phase in model B for $T < 115$ K corresponds to an inhomogeneous phase made up of a small amount of crystalline atoms and amorphous (liquid or solid) atoms.

Further molecular simulations are needed to corroborate and complete the present study. Starting from well-equilibrated configurations of confined argon in the disordered porous material, we will investigate the dynamics of the confined phase using molecular dynamics simulations. This will provide useful information regarding the nature of the confined phase, such as its diffusion coefficient and relaxation time. From an experimental point of view, ^{1}H-NMR and scattering experiments can be used to corroborate our findings.

ACKNOWLEDGMENTS

We wish to thank Christiane Alba-Simionesco, Gilberte Dosseh, Francisco R. Hung, Roland J.-M. Pellenq, and José Teixeira for very helpful discussions. We thank the National Science Foundation (Grant No. CTS-0626031) and the U.S. Department of Energy (Grant No. DE-FG02-98ER14847) for funding. This research was performed using supercomputing resources from San Diego Supercomputer Center (NSF/MRAC-CHE050047S), the High Performance Computing Center at North Carolina State University, and the Centre Informatique National de l'Enseignement Superieur at Montpellier (CMC 2017).

*Corresponding author. bcoasne@lpmc.univ-montp2.fr; FAX: +33 4 67 14 42 90.

[1] R. C. Bansal, J. B. Donnet, and F. Stoeckli, *Active Carbon* (Marcel Dekker, New York, 1988).
[2] S. Sircar, T. C. Golden, and M. B. Rao, Carbon **34**, 1 (1996).
[3] F. Rouquerol, J. Rouquerol, and K. S. W. Sing, *Adsorption by Powders and Porous Solids* (Academic Press, London, 1999).
[4] T. J. Bandosz, M. J. Biggs, K. E. Gubbins, Y. Hattori, T. Liyama, K. Kaneko, J. P. Pikunic, and K. T. Thomson, Chem. Phys. Carbon **8**, 41 (2003).
[5] B. McEnaney, Carbon **26**, 267 (1988).
[6] H. Marsh and P. L. Walker, Jr., *Chemistry and Physics of Carbon* (Marcel Dekker, New York, 1979), Vol. 15, Chap. 3.
[7] T. J. Mays, *Carbon Materials for Advanced Technologies* (Pergamon, Amsterdam, 1999), Chap. 3.
[8] Z. H. Huang, F. Kang, W. Huang, J. B. Yang, K. M. Liang, M. L. Cui, and Z. Cheng, J. Colloid Interface Sci. **249**, 453 (2002).
[9] J. P. Pikunic, C. Clinard, N. Cohaut, K. E. Gubbins, J. M. Guet, R. J. M. Pellenq, I. Rannou, and J. -N. Rouzaud, Langmuir **19**, 8565 (2003).
[10] L. D. Gelb, K. E. Gubbins, R. Radhakrishnan, and M. Sliwinska-Bartkowiak, Rep. Prog. Phys. **62**, 1573 (1999).
[11] C. Alba-Simionesco, B. Coasne, G. Dosseh, G. Dudziak, K. E. Gubbins, R. Radhakrishnan, and M. Sliwinska-Bartkowiak, J. Phys.: Condens. Matter **18**, R15 (2006).
[12] A. Striolo, K. E. Gubbins, A. A. Chialvo, and P. T. Cummings, Adsorption **11**, 337 (2005).
[13] B. Coasne, J. P. Pikunic, R. J. M. Pellenq, and K. E. Gubbins, Mater. Res. Soc. Symp. Proc. **790**, P8.5 (2003).
[14] M. J. Biggs, A. Buts, and D. Williamson, Langmuir **20**, 5786 (2004).
[15] S. K. Jain, J. P. Pikunic, R. J. M. Pellenq, and K. E. Gubbins, Adsorption **11**, 355 (2005).
[16] J. P. Pikunic, P. Llewellyn, R. J. M. Pellenq, and K. E. Gubbins, Langmuir **21**, 4431 (2005).
[17] B. Coasne, K. E. Gubbins, F. R. Hung, and S. K. Jain, Mol. Simul. **32**, 557 (2006).
[18] B. Coasne, S. K. Jain, and K. E. Gubbins, Mol. Phys. **104**, 3491 (2006).
[19] B. Coasne, A. Grosman, C. Ortega, and R. J. M. Pellenq, Stud. Surf. Sci. Catal. **144**, 35 (2002).
[20] Y. He and N. A. Seaton, Langmuir **19**, 10132 (2003).
[21] B. Coasne and R. J. M. Pellenq, J. Chem. Phys. **120**, 2913 (2004).
[22] B. Coasne and R. J. M. Pellenq, J. Chem. Phys. **121**, 3767 (2004).
[23] B. Coasne, K. E. Gubbins, and R. J. M. Pellenq, Part. Part. Syst. Charact. **21**, 149 (2004).
[24] B. Coasne, F. R. Hung, F. R. Siperstein, and K. E. Gubbins, Ann. Chim. (Paris) **30**, 375 (2005).
[25] B. Coasne, F. R. Hung, R. J. M. Pellenq, F. R. Siperstein, and K. E. Gubbins, Langmuir **22**, 194 (2006).
[26] F. R. Hung, B. Coasne, K. E. Gubbins, F. R. Siperstein, and M. Sliwinska-Bartkowiak, Stud. Surf. Sci. Catal. **160**, 153 (2006).
[27] F. R. Hung, B. Coasne, E. E. Santiso, K. E. Gubbins, F. R. Siperstein, and M. Sliwinska-Bartkowiak, J. Chem. Phys. **122**, 144706 (2005).
[28] A. Oberlin, S. Bonnamy, and P. G. Rouxhet, Chem. Phys. Carbon **26**, 1 (1999).
[29] A. Oberlin, Chem. Phys. Carbon **22**, 1 (1989).

[30] R. L. McGreevy and L. Pusztai, Mol. Simul. **1**, 359 (1988).
[31] K. T. Thomson and K. E. Gubbins, Langmuir **16**, 5761 (2000).
[32] S. K. Jain, J. Fuhr, R. J. M. Pellenq, J. P. Pikunic, C. Bichara, and K. E. Gubbins, Stud. Surf. Sci. Catal. **160**, 169 (2006).
[33] B. Coasne, S. K. Jain, and K. E. Gubbins, Phys. Rev. Lett. **97**, 105702 (2006); **97**, 105702(E) (2006).
[34] W. A. Steele, Surf. Sci. **36**, 317 (1973).
[35] W. A. Steele, *The Interaction of Gases with Solid Surfaces* (Pergamon Press, Oxford, 1974).
[36] W. B. Streett and L. A. K. Staveley, J. Chem. Phys. **47**, 2449 (1967).
[37] J. S. Rowlinson, *Liquids and Liquid Mixtures* (Butterworth Scientific, London, 1982).
[38] R. Radhakrishnan, K. E. Gubbins, and M. Sliwinska-Bartkowiak, J. Chem. Phys. **112**, 11048 (2000).
[39] R. Radhakrishnan, K. E. Gubbins, and M. Sliwinska-Bartkowiak, J. Chem. Phys. **116**, 1147 (2002).
[40] R. L. Henderson, Phys. Lett. **49A**, 197 (1974); C. G. Gray and K. E. Gubbins, *Theory of Molecular Fluids* (Clarendon Press, Oxford, 1984), p. 178.
[41] R. Evans, Mol. Simul. **4**, 409 (1990).
[42] L. D. Gelb and K. E. Gubbins, Langmuir **15**, 305 (1999).
[43] D. Nicholson and N. G. Parsonage, *Computer Simulation and the Statistical Mechanics of Adsorption* (Academic Press, New York, 1982).
[44] M. P. Allen and D. J. Tildesley, *Computer Simulation of Liquids* (Oxford, Clarendon, 1987).
[45] D. Frenkel and B. Smit, *Understanding Molecular Simulation: From Algorithms to Applications*, 2nd ed. (Academic Press, London, 2002).
[46] R. J. M. Pellenq and D. Nicholson, Langmuir **11**, 1626 (1995).
[47] L. D. Gelb and K. E. Gubbins, Langmuir **14**, 2097 (1998).
[48] B. Coasne, F. Di Renzo, A. Galarneau, and R. J. M. Pellenq, Langmuir **22**, 11097 (2006).
[49] R. J. M. Pellenq and P. E. Levitz, Mol. Simul. **27**, 353 (2001).
[50] Q. L. Yan and J. J. de Pablo, J. Chem. Phys. **111**, 9509 (1999).
[51] R. Faller, Q. L. Yan, and J. J. de Pablo, J. Chem. Phys. **116**, 5419 (2002).
[52] B. Coasne, J. Czwartos, K. E. Gubbins, F. R. Hung, and M. Sliwinska-Bartkowiak, Mol. Phys. **102**, 2149 (2004).
[53] B. Coasne, J. Czwartos, K. E. Gubbins, F. R. Hung, and M. Sliwinska-Bartkowiak, Adsorption **11**, 301 (2005).
[54] E. Marinari and G. Parisi, Europhys. Lett. **191**, 451 (1992).
[55] Q. L. Yan and J. J. de Pablo, J. Chem. Phys. **113**, 1276 (2000).
[56] M. Sliwinska-Bartkowiak, F. R. Hung, E. E. Santiso, B. Coasne, G. Dudziak, F. R. Siperstein, and K. E. Gubbins, Adsorption **11**, 391 (2005).
[57] R. Radhakrishnan and K. E. Gubbins, Mol. Phys. **96**, 1249 (1999).
[58] F. R. Hung, G. Dudziak, M. Sliwinska-Bartkowiak, and K. E. Gubbins, Mol. Phys. **102**, 223 (2004).
[59] B. I. Halperin and D. R. Nelson, Phys. Rev. Lett. **41**, 121 (1978); D. R. Nelson and B. I. Halperin, Phys. Rev. B **19**, 2457 (1979); A. P. Young, *ibid.* **19**, 1855 (1979).
[60] K. J. Strandburg, Rev. Mod. Phys. **60**, 161 (1988).
[61] M. Miyahara and K. E. Gubbins, J. Chem. Phys. **106**, 2865 (1997).
[62] P. J. Steinhardt, D. R. Nelson, and M. Ronchetti, Phys. Rev. B **28**, 784 (1983).
[63] C. G. Gray and K. E. Gubbins, *Theory of Molecular Liquids* (Clarendon Press, Oxford, 1984).
[64] J. S. van Duijneveldt and D. Frenkel, J. Chem. Phys. **96**, 4655 (1992).
[65] R. M. Lynden-Bell, J. S. van Duijneveldt, and D. Frenkel, Mol. Phys. **80**, 801 (1993).
[66] P. R. ten Wolde, M. J. Ruiz-Montero, and D. Frenkel, J. Chem. Phys. **104**, 9932 (1996).
[67] R. Radhakrishnan, K. E. Gubbins, A. Watanabe, and K. Kaneko, J. Chem. Phys. **111**, 9058 (1999).
[68] J. Czwartos, B. Coasne, K. E. Gubbins, F. R. Hung, and M. Sliwinska-Bartkowiak, Mol. Phys. **103**, 3103 (2005).
[69] R. Radhakrishnan, K. E. Gubbins, and M. Sliwinska-Bartkowiak, Phys. Rev. Lett. **89**, 076101 (2002).
[70] R. Radhakrishnan, K. E. Gubbins, and M. Sliwinska-Bartkowiak (unpublished).
[71] J. M. Kosterlitz and D. J. Thouless, J. Phys. C **5**, L124 (1972).
[72] J. M. Kosterlitz and D. J. Thouless, J. Phys. C **6**, 1181 (1973).
[73] J. Warnock, D. D. Awschalom, and M. W. Shafer, Phys. Rev. Lett. **57**, 1753 (1986).
[74] R. Evans and U. Marini Bettolo Marconi, J. Chem. Phys. **86**, 7138 (1987).
[75] M. Sliwinska-Bartkowiak, G. Dudziak, R. Sikorski, R. Gras, R. Radhakrishnan, and K. E. Gubbins, J. Chem. Phys. **114**, 950 (2001).
[76] K. Morishige and H. Iwasaki, Langmuir **19**, 2808 (2003).